

Research Article

Le Thi Duyen*, Le Thi Phuong Thao, and Bui Hoang Bac

Research on the adsorption of Co^{2+} ions using halloysite clay and the ability to recover them by electrodeposition method

<https://doi.org/10.1515/gps-2023-0160>

received August 27, 2023; accepted January 2, 2024

Abstract: In environmental research, along with discovering methods for adsorbing heavy metals, it is essential to comprehend the processes of desorption and recovery of these heavy metals from adsorbent materials and their reuse. In this study, halloysite (HAL) clay, obtained from the Thach Khoan, Vietnam, was utilized for the removal of Co^{2+} ions from an aqueous solution, and the influence of different factors on the adsorption properties of Co^{2+} was investigated. Optimal conditions determined were 0.8 g HAL mass per 50 mL of solution, initial Co^{2+} concentration of $40 \text{ mg}\cdot\text{L}^{-1}$, contact time of 80 min, pH_0 of 6.09, and room temperature of 30°C . Under these conditions, the adsorption efficiency and capacity obtained were $76.358 \pm 0.981\%$ and $1.909 \pm 0.025 \text{ mg}\cdot\text{g}^{-1}$, respectively. The adsorption process followed the Langmuir adsorption isotherms, with a maximum monolayer adsorption capacity of $3.10206 \pm 0.13551 \text{ mg}\cdot\text{g}^{-1}$, and exhibited a pseudo-second-order kinetic model. Desorption experiments were conducted using the electrochemical method with a deep eutectic solvent based on choline chloride and urea (reline). The results demonstrated that 94.11% of the Co metal could be recovered through electrodeposition after 5 h, using an applied current of 7.5 mA at 60°C . The HAL material was successfully regenerated following the desorption process.

Keywords: halloysite, adsorption, desorption, recovery, electrodeposition, Co^{2+} , ion

1 Introduction

Halloysite (HAL) belongs to the kaolin mineral group, which includes minerals such as kaolinite, dickite, nacrite, and HAL itself. HAL occurs in two main polymorphs: a fully hydrated form with the chemical formula $\text{Al}_2\text{Si}_2\text{O}_5(\text{OH})_4\cdot 2\text{H}_2\text{O}$ and a dehydrated form with the chemical formula $\text{Al}_2\text{Si}_2\text{O}_5(\text{OH})_4$ [1]. HAL can exhibit various morphological forms, including tubular, spherical, and layered structures. In recent years, HAL has gained significant attention from scientists due to its unique properties, such as its tubular structure, non-toxicity, large surface area, high mechanical strength, and cost-effectiveness compared to nanotubular carbon. As a result, HAL has found applications in various fields, including pharmaceuticals, medicine, food, high-grade materials, agriculture, and environmental applications [2,3]. In particular, HAL has proven to be an effective adsorbent for heavy metals [4–12].

Among the various methods available for treating water pollution caused by heavy metals, adsorption has emerged as a promising approach due to its simplicity, effectiveness, and broad applicability. In adsorption, the choice of adsorbent material plays a crucial role. Many studies have focused on utilizing natural and environmentally friendly materials as adsorbents for heavy metal removal. Cellulose has been investigated as an adsorbent for heavy metal removal [13,14]. Similarly, chitosan has shown promise in adsorbing heavy metals [15,16]. Hydroxyapatite [17], montmorillonite [18], natural clay [19], and plant straw [20] have also been explored as effective adsorbents for heavy metal adsorption.

There has been extensive research on heavy metal adsorption from the environment and industrial wastewater. However, studies focusing on the desorption and recovery of heavy metals from adsorbed materials and the regeneration of adsorbents for subsequent adsorption processes have received limited attention. Yet, the desorption of heavy metals from adsorbed materials is crucial to prevent secondary pollution and to enable the reuse of

* **Corresponding author: Le Thi Duyen**, Department of Chemistry, Faculty of Basic Science, Hanoi University of Mining and Geology, Hanoi, Vietnam; HiTech-CEAE Research Team, Hanoi University of Mining and Geology, Hanoi, Vietnam, e-mail: lethiduyen@humg.edu.vn

Le Thi Phuong Thao: Department of Chemistry, Faculty of Basic Science, Hanoi University of Mining and Geology, Hanoi, Vietnam; HiTech-CEAE Research Team, Hanoi University of Mining and Geology, Hanoi, Vietnam

Bui Hoang Bac: Faculty of Geosciences and Geology Engineering, Hanoi University of Mining and Geology, Hanoi, Vietnam; HiTech-CEAE Research Team, Hanoi University of Mining and Geology, Hanoi, Vietnam; Innovations for Sustainable and Responsible Mining (ISRM) Research Group, Hanoi University of Mining and Geology, Hanoi, Vietnam

materials. Although some studies have been published on the desorption and recovery of heavy metals from hydroxyapatite [21–27] and clays [28–30], there are few published studies specifically addressing the desorption, recovery, and reuse of heavy metals from HAL [9,10,28]. For instance, Itami and Yanai investigated the sorption/desorption properties of Cd and Cu on five clay types, highlighting the influence of the clays' charge characteristics and pH [28]. Another study by Helios Rybicka *et al.* examined the adsorption/desorption behavior of Cd, Cu, Pb, Zn, and Ni on illite, beidellite, and montmorillonite. The results showed that the adsorption capacity of the clays was higher for Pb and Cu ions than for Ni, Zn, and Cd ions. Furthermore, the desorption properties varied, with $Pb > Cd > Cu > Ni > Zn$ for beidellite and $Pb > Cd \sim Cu > Ni > Zn$ for illite and montmorillonite using $NaNO_3$ as the eluent agent [29].

Cobalt is an essential trace element that is naturally present in all organs and cells of the body. It plays a vital role in synthesizing vitamin B12 and certain enzymes. However, excessive cobalt absorption at high concentrations can pose severe risks to humans, animals, and plants. Exposure to elevated levels of cobalt can lead to respiratory symptoms, lung damage, hypothyroidism, dermatitis, heart disease, and hearing and vision loss, among other health issues. Studies have demonstrated that plant mortality can occur when the cobalt concentration in the soil solution exceeds $10 \text{ mg}\cdot\text{L}^{-1}$.

Similarly, fish can die when the cobalt concentration in water surpasses $5 \text{ mg}\cdot\text{L}^{-1}$. To regulate and maintain safe levels, the Food and Agriculture Organization of the United Nations has set guidelines specifying that the cobalt content in irrigation water should not exceed $100 \text{ }\mu\text{g}\cdot\text{L}^{-1}$, and the concentration of cobalt ions in wastewater must be kept below $1.0 \text{ mg}\cdot\text{L}^{-1}$ [31]. These guidelines safeguard organisms' health and mitigate the potential adverse effects of elevated cobalt concentrations.

Indeed, cobalt adsorption has been a subject of interest and research using various adsorbent materials. Different types of adsorbents have shown positive results in treating cobalt in water. Activated carbons produced from waste potato peels were also utilized for $Co(II)$ adsorption from synthetic water. The resulting carbon materials had different surface areas depending on the processing temperature, and the maximum adsorption capacity reached up to $405 \text{ mg}\cdot\text{g}^{-1}$ at an optimum pH of 6 [32]. The combination of HAL and cellulose into polyurethane foam also improved the adsorption capacity of the foam to metal ions in the solution. Various functional groups in HAL and cellulose contributed to electrostatic bonds between the adsorbent and metal ions, leading to increased adsorption capacity

[33]. However, despite these promising results with other metals, fewer reports have been published specifically on $Co(II)$ adsorption using HAL. This indicates the need for more research to explore and optimize the potential of HAL as an effective adsorbent for cobalt ions.

In this study, we aim to adsorb Co^{2+} ions using HAL clay as the adsorbent material. Subsequently, we focus on the desorption and recovery of cobalt from the adsorbed HAL material using an electrolysis process in a reline electrolyte, a non-toxic deep eutectic solvent (DES). DESs have gained attention in recent years. These solvents can be easily formed by mixing two safe components that are cost-effective, renewable, and biodegradable, capable of creating a eutectic mixture. Choline chloride (ChCl) is a commonly used component for generating DESs. Several publications have reported successful cobalt deposition from DESs formed with ChCl [34–37]. Our study's main advantage lies in performing cobalt's desorption and recovery process simultaneously within an electrochemical cell. This approach allows for the reuse of the HAL adsorbent, minimizing waste and maximizing the efficiency of cobalt recovery.

2 Experimental method

2.1 Preparation of HAL powder

The HAL material was collected from the Lang Dong mine in Phu Tho province, Vietnam. After collection, the sample was mixed thoroughly and separated using the wet sieving method to achieve a particle size of less than $32 \text{ }\mu\text{m}$. The separated sample with a particle size of $<32 \text{ }\mu\text{m}$ was then dried at 60°C and finely ground using an agate mortar. The resulting HAL powder was used for subsequent analysis and experiments.

2.2 Preparation of DES

The DESs used in the study were prepared by mixing ChCl (Alfa Aesar, purity $\geq 98\%$) and urea (U; VWR Chemicals, NORMAPUR). ChCl was recrystallized from absolute ethanol (VWR Chemicals, NORMAPUR), followed by filtration and drying under vacuum. ChCl and U were then combined in a 1:2 molar ratio within a closed container. The mixture was stirred continuously for 3 h at 60°C until a homogeneous colorless liquid, known as ChCl-U (Reline) DES, was formed.

2.3 Determination of pH_{PZC} of HAL powder

A mixture of 0.5 g HAL powder was combined with 50.0 mL of 0.01 M KNO_3 solution. The mixture was stirred for 60 min at room temperature. To adjust the initial pH values (pH_0), either a 0.1 M KOH solution or a 0.1 M HNO_3 solution was used within a pH range of 2.5–9.5. Once the equilibrium was reached, the pH values were measured again (pH_f). The point of zero charge (pH_{PZC}) was determined from the $\Delta\text{pH} = f(\text{pH}_0)$ plot, where ΔpH represents the difference between pH_0 and pH_f . The pH_{PZC} corresponds to the pH_0 value when ΔpH equals zero.

2.4 Adsorption experiments

The experiments were conducted at room temperature with continuous stirring at 400 rpm, a contact time studied from 10 to 120 min, pH from 2.37 to 6.99, mass of HAL changed from 0.3 to 1.2 g, initial concentration of Co^{2+} verified between 10 and 80 $\text{mg}\cdot\text{L}^{-1}$. After the adsorption process, the solution was filtered to remove the solid HAL material, and the remaining concentration of Co^{2+} was determined using the Inductively coupled plasma mass spectrometry (ICP-MS) method on ICAP Q ICP-MS (Thermo Scientific, Germany) instrument.

The adsorption capacity and efficiency were calculated using Eqs. 1 and 2, respectively [38] as follows:

$$Q = (C_0 - C) \times V/m \quad (1)$$

$$H = (C_0 - C) \times 100/C_0 \quad (2)$$

The amount of metal ion adsorbed on the adsorbent at equilibrium (Q) is calculated using the equation $Q = (C_0 - C) \times V/m$, where C_0 and C represent the initial and equilibrium concentrations ($\text{mg}\cdot\text{L}^{-1}$) of Co^{2+} ions in the solution, respectively. V denotes the volume of the solution (L), and m is the mass of the adsorbent (g).

The experimental data obtained are analyzed using the Langmuir and Freundlich isotherm models [39].

Langmuir non-linear equation:

$$Q_e = Q_m \cdot \frac{K_L \cdot C_e}{1 + K_L \cdot C_e} \quad (3)$$

Freundlich non-linear equation:

$$Q_e = K_F \cdot C_e^{1/n} \quad (4)$$

where C_e ($\text{mg}\cdot\text{L}^{-1}$) is the equilibrium concentration of Co^{2+} , Q ($\text{mg}\cdot\text{g}^{-1}$) is the amount adsorbed at equilibrium, Q_m ($\text{mg}\cdot\text{g}^{-1}$) is the maximum adsorption capacity, K_L is the Langmuir coefficient related to the adsorption energy, K_F and n are the constants of the Freundlich model.

The adsorption kinetics is described by the pseudo-first-order and pseudo-second-order kinetic models using Eqs. 5 and 6, respectively [40].

$$Q_t = Q_e \cdot (1 - e^{-k_1 t}) \quad (5)$$

$$Q_e = \frac{k_2 \cdot Q_e^2 \cdot t}{1 + k_2 \cdot Q_e \cdot t} \quad (6)$$

where Q_e is the adsorption capacity at equilibrium ($\text{mg}\cdot\text{g}^{-1}$), Q_t is the adsorption capacity at time t ($\text{mg}\cdot\text{g}^{-1}$), and k_1 and k_2 are the pseudo-first-order ($\text{min}\cdot\text{L}$) and pseudo-second-order ($\text{g}\cdot\text{mg}^{-1}\cdot\text{min}^{-1}$) rate constants, respectively.

Physicochemical characteristics of HAL before and after Co^{2+} adsorption were analyzed by the following methods: The phase component was analyzed using X-ray diffraction (XRD) (Siemens D5000 diffractometer, $\text{CuK}\alpha$ radiation, $\lambda = 1.54056 \text{ \AA}$, with a step angle of 0.030° , scanning rate of $0.04285^\circ\cdot\text{s}^{-1}$, and 2θ in the range of $20\text{--}70^\circ$). The structure was analyzed by infrared spectroscopy (FT-IR) on a Nicolet iS10 instrument (Thermo Scientific, USA). Morphology and element components were analyzed by SEM-EDX on a FE-SEM-JSM-IT800 instrument (JEOL, Japan).

2.5 Electrochemistry experiments for desorption and recovery cobalt

2.5.1 Cyclic voltammetry scan in reline solvent

In the cyclic voltammetry scan experiments, a three-electrode system was used, and it was connected to an Autolab PGSTAT20 potentiostat from Metrohm. The working electrode (WE) used was a gold (Au) electrode with a geometric area of 0.0201 cm^2 . The reference electrode (RE) was an Ag/AgCl electrode with a chloride-ion-saturated potassium chloride solution ($\text{Ag, AgCl}|\text{Cl}^-$), and the counter electrode (CE) was a platinum grid with a large area. A sample volume of 5 mL of reline DES containing either 0.5 g of $\text{Co}(\text{NO}_3)_2$ or 0.5 g of Co-HAL was used for the experiments. The scan potential range was set from -0.2 to -1.5 V , and the scan rate was $50 \text{ mV}\cdot\text{s}^{-1}$. The experiments were carried out at a temperature of 60°C . Before the experiments, the WE (Au electrode) was polished using an alumina-water slurry on a smooth polishing cloth. It was then sonicated twice for 3 min and rinsed with Milli-Q water to ensure no remaining alumina. Finally, it was dried under a nitrogen atmosphere. The platinum CE was cleaned by flaming it until it reached a red glow. Before each experiment, the DES medium was purged with nitrogen for at least 20 min, and during all measurements, the system was kept under a nitrogen atmosphere. This careful preparation and control

of the experimental conditions ensured accurate and reliable results during the cyclic voltammetry scans in the reline DES.

2.5.2 Desorption of Co^{2+} and deposition of Co metal on the surface of an electrode

The desorption of Co^{2+} from Co-HAL and the subsequent electrodeposition of Co metal were performed in a three-electrode electrochemical cell. The WE used was a gold plate with a geometric area of 1 cm^2 . The RE used was Ag/AgCl with a chloride-ion-saturated potassium chloride solution (Ag, AgCl|Cl⁻), and the CE was a platinum grid with a large area. Cobalt recovery was carried out using the electrodeposition method in the reline solvent. The deposition potential was set to be less than or equal to -1.3 V , and the temperature was maintained at 60°C . Before starting the electrolysis process, the DES medium was purged with nitrogen for at least 20 min, and the nitrogen atmosphere was maintained throughout the electrolysis. Different applied current values of 1, 2, 3, 5, and 7.5 mA were used, and the electrolytic time was varied from 1 to 5 h. After the electrolysis process, the Co-HAL powder was filtered out from the mixture. Then, it underwent cleaning, drying, and the remaining Co in the powder was determined by the ICP-MS method.

The surface of the Au electrode before and after electrolysis was analyzed by SEM-EDX. The phase component of initial HAL and reused HAL after the desorption process of Co^{2+} were analyzed using XRD.

3 Results and discussion

3.1 Effect of the experimental factors on Co^{2+} ions adsorption by HAL powder

3.1.1 pH_{PZC} of HAL

The change in ΔpH against pH_0 is presented in Figure 1. Based on the graph, it can be observed that ΔpH equals zero when the pH_0 value is 5.99. This indicates that the point of zero charge (pH_{PZC}) for the HAL material used in the study is determined to be 5.99. The pH_{PZC} represents the pH value at which the surface charge of the material is neutral, indicating that the material has no net positive or negative charge.

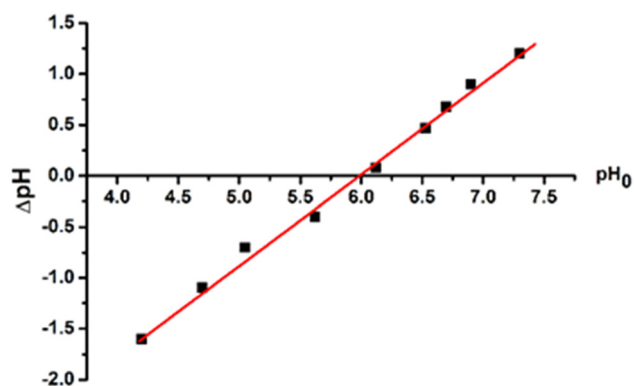


Figure 1: Determination of pH_{PZC} of HAL powder.

3.1.2 Effect of contact time

The contact time between the solid adsorbent (HAL) and the metal ion solution (Co^{2+}) plays a crucial role in adsorption. To investigate the influence of contact time on HAL's adsorption ability for Co^{2+} ions, experiments were conducted for 10–120 min using a $50\text{ mg}\cdot\text{L}^{-1}$ Co^{2+} solution. As shown in Table 1, the results indicate that as the contact time increased, the adsorption capacity and efficiency of the HAL for Co^{2+} ions gradually increased. However, once the contact time reached 80 min, the adsorption capacity and efficiency became nearly stable. This suggests that after 80 min, the adsorption process of Co^{2+} ions by HAL reached equilibrium, with no significant further increase in adsorption. Based on these findings, a contact time of 80 min was chosen for subsequent studies, representing the time required to achieve equilibrium in the Co^{2+} adsorption process by HAL.

3.1.3 Effect of solution pH

The effect of pH on the Co^{2+} adsorption capacity of HAL was investigated because changes in solution pH can influence the surface properties of the adsorbent and the form of metal ions in the solution. The study was conducted with the Co^{2+} solution having a concentration of $50\text{ mg}\cdot\text{L}^{-1}$, and the pH values were varied around the pH_{PZC} value of HAL, which was determined to be 5.99. However, it is essential to note that precipitation of Co^{2+} hydroxide starts to occur at a pH of 7.8 [41]. To accurately assess the amount of ion depletion in the solution due to adsorption on HAL, the pH was controlled to be less than 7.8. As shown in Table 2, the results demonstrated that within the investigated pH

Table 1: Effect of contact time on the HAL's adsorption of Co^{2+} at an initial concentration of $50 \text{ mg}\cdot\text{L}^{-1}$, HAL dosage 0.5 g , and $\text{pH} = 6.09$

t (min)	C_e ($\text{mg}\cdot\text{L}^{-1}$)	$H\%$	Q ($\text{mg}\cdot\text{g}^{-1}$)
10	28.780 ± 0.514	42.441 ± 1.027	2.122 ± 0.051
20	27.561 ± 0.818	44.878 ± 1.636	2.244 ± 0.082
30	26.170 ± 0.314	47.660 ± 0.629	2.383 ± 0.031
40	25.670 ± 0.401	48.660 ± 0.802	2.433 ± 0.040
50	24.923 ± 0.545	50.155 ± 1.090	2.508 ± 0.055
60	24.452 ± 0.620	51.096 ± 1.241	2.555 ± 0.062
80	24.333 ± 0.496	51.334 ± 0.991	2.567 ± 0.050
100	24.226 ± 0.430	51.548 ± 0.860	2.577 ± 0.043
120	24.205 ± 0.575	51.590 ± 1.150	2.580 ± 0.058

range, both the adsorption efficiency and capacity of Co^{2+} ions by HAL increased as the pH increased. This can be explained by the protonation of HAL in acidic environments, resulting in a positively charged surface. Consequently, the number of adsorption sites for positive ions on HAL decreased, and competitive adsorption occurred between H^+ ions and Co^{2+} ions on the surface of HAL, leading to a decrease in the adsorption ability of Co^{2+} ions [40]. As the pH increased, the positive charge density on the surface of HAL decreased, thereby enhancing the adsorption capacity of Co^{2+} ions. Favorable adsorption of Co^{2+} ions occurred when the pH was higher than the pH_{PZC} value of HAL. To facilitate the treatment of larger quantities without the need for pH adjustment, an initial pH of 6.09 was selected for Co^{2+} adsorption in subsequent studies. The adsorption efficiency and capacity reached $51.334 \pm 1.047\%$ and $2.567 \pm 0.052 \text{ mg}\cdot\text{g}^{-1}$ at this pH, respectively.

3.1.4 Effect of material mass

When the mass of the solid adsorbent in the solution increases, the contact area between the adsorbent and the solution also increases. This increases the number of

Table 2: Effect of pH on the HAL's adsorption of Co^{2+} at an initial concentration of $50 \text{ mg}\cdot\text{L}^{-1}$, HAL dosage of 0.5 g , and contact time of 80 min

t (min)	C_e ($\text{mg}\cdot\text{L}^{-1}$)	$H\%$	Q ($\text{mg}\cdot\text{g}^{-1}$)
2.37	41.803 ± 0.022	16.394 ± 0.043	0.820 ± 0.002
2.95	37.610 ± 0.466	24.780 ± 0.932	1.239 ± 0.047
4.11	32.850 ± 0.463	34.300 ± 0.925	1.715 ± 0.046
5.02	28.580 ± 0.521	42.840 ± 1.042	2.142 ± 0.052
6.09	24.333 ± 0.524	51.334 ± 1.047	2.567 ± 0.052
6.50	21.356 ± 0.607	57.288 ± 1.214	2.864 ± 0.061
6.99	18.661 ± 0.733	62.678 ± 1.466	3.134 ± 0.073

active sites available for adsorption, resulting in higher adsorption efficiency [41]. This study observed that adsorption efficiency increased rapidly from $45.405 \pm 0.824\%$ to $71.308 \pm 0.925\%$ as the mass of HAL increased from 0.3 to 0.8 g (Figure 2). After reaching 0.8 g , further increases in the amount of adsorbent resulted in only slight improvements in adsorption efficiency. This is because the adsorption process reached equilibrium, and additional adsorbent did not significantly impact the overall efficiency. To achieve an appropriate magnitude of adsorption capacity and efficiency ($2.228 \pm 0.029 \text{ mg}\cdot\text{g}^{-1}$ and $71.308 \pm 0.925\%$, respectively), a mass of 0.8 g of HAL was selected to study the adsorption of Co^{2+} ions. This mass provided optimal adsorption performance, balancing the amount of adsorbent with the achieved efficiency.

3.1.5 Effect of Co^{2+} concentration

The investigation of the adsorption process with varying initial concentrations of Co^{2+} ions (20 – $80 \text{ mg}\cdot\text{L}^{-1}$) revealed significant findings, as shown in Table 3 and Figure 3. As the concentration of Co^{2+} ions increased, the adsorption capacity of HAL gradually increased while the adsorption efficiency decreased. For low initial concentrations of Co^{2+} ions, the adsorption of Co^{2+} onto HAL was favorable due to the large contact area between the Co^{2+} ions and the solid phase of HAL. However, as the initial concentration of Co^{2+} ions increased, the amount of Co^{2+} ions also increased. Nevertheless, the adsorption capacity of HAL reached saturation and did not increase further, resulting in a decrease in the adsorption efficiency [42]. To achieve a high simultaneous

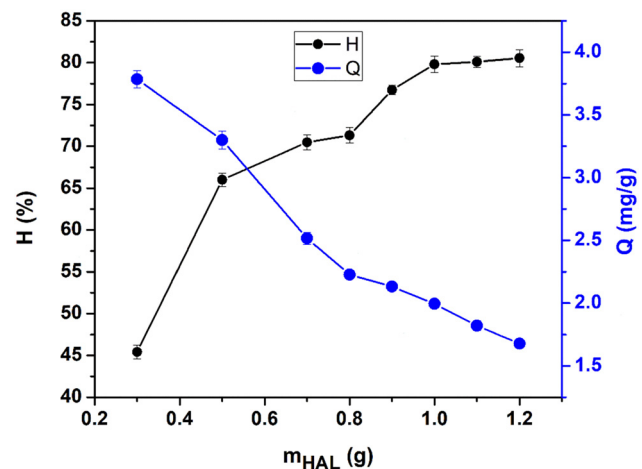
**Figure 2:** The effect of material mass on the HAL's adsorption of Co^{2+} at an initial concentration of $50 \text{ mg}\cdot\text{L}^{-1}$, $\text{pH} = 6.09$, and contact time of 80 min .

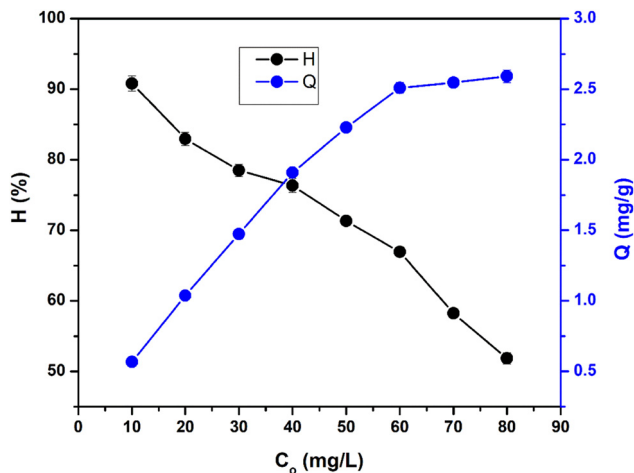
Table 3: Values of $H\%$ and Q ($\text{mg}\cdot\text{g}^{-1}$) were calculated from the different initial concentrations of Co^{2+}

C_o ($\text{mg}\cdot\text{L}^{-1}$)	C_e ($\text{mg}\cdot\text{L}^{-1}$)	$H\%$	Q ($\text{mg}\cdot\text{g}^{-1}$)
10	0.918	90.820 ± 1.052	0.568 ± 0.016
20	3.408	82.960 ± 0.937	1.037 ± 0.021
30	6.45	78.500 ± 0.864	1.472 ± 0.034
40	9.457	76.358 ± 0.981	1.909 ± 0.025
50	14.346	71.308 ± 0.653	2.228 ± 0.032
60	19.842	66.930 ± 0.724	2.510 ± 0.038
70	29.251	58.213 ± 0.582	2.547 ± 0.029
80	38.523	51.846 ± 0.806	2.592 ± 0.045

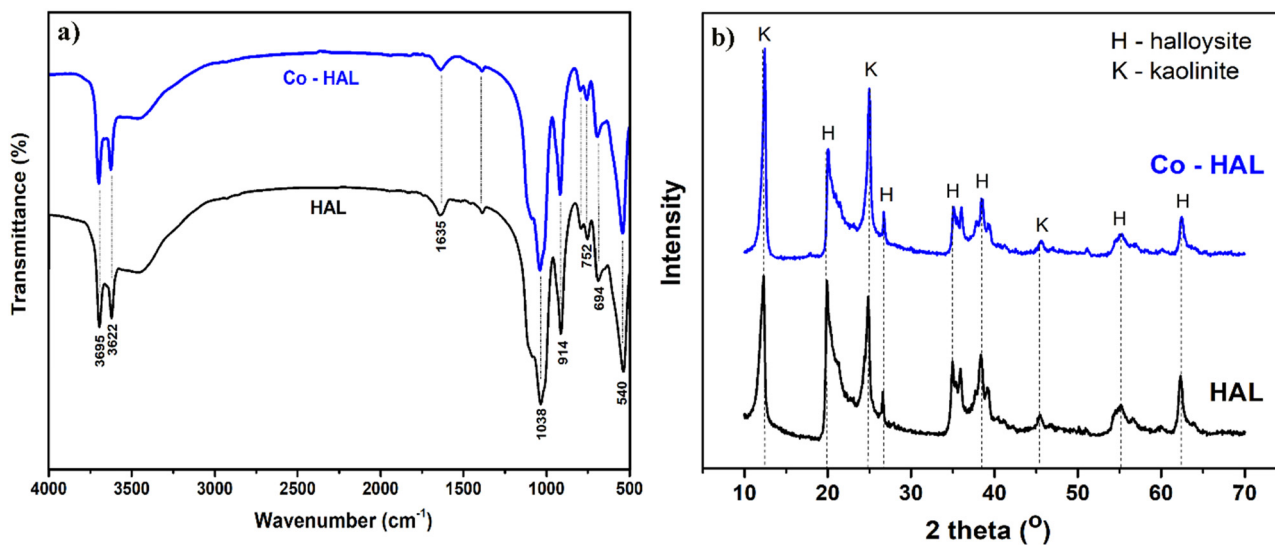
adsorption capacity and efficiency, an appropriate concentration of Co^{2+} ions was selected within the range of $30\text{--}50\text{ mg}\cdot\text{L}^{-1}$. At a concentration of $40\text{ mg}\cdot\text{L}^{-1}$ of Co^{2+} ions, HAL's adsorption efficiency and capacity reached $76.358 \pm 0.981\%$ and $1.909 \pm 0.025\text{ mg}\cdot\text{g}^{-1}$, respectively. This result is considered acceptable when comparing the adsorption efficiency of HAL for Co^{2+} ions with other investigated metal ions, such as Cd^{2+} with an efficiency of 51.45% and Pb^{2+} with an efficiency of 79.3% [43], as well as $\text{As}(\text{m})$ with an efficiency of 82.4% [42].

3.1.6 Characterization of HAL before and after adsorption process

The HAL powder before and after Co^{2+} adsorption was characterized through FT-IR, XRD, and SEM-EDX analyses (Figures 4 and 5). It can be observed that the FT-IR and XRD analysis graphs for both types of samples are similar and show no significant changes. The FT-IR spectra exhibit

**Figure 3:** The effect of Co^{2+} concentration on the HAL's adsorption of Co^{2+} at a dosage 0.8 g , $\text{pH} = 6.09$, and contact time of 80 min .

vibrations of O–H groups on the inner surface (at $3,695$ and $3,622\text{ cm}^{-1}$), interlayer water (at $1,635\text{ cm}^{-1}$), Si–O (at $1,038$ and 694 cm^{-1}), Al–OH (at 914 cm^{-1}), Al–O–OH (at 796 , 752 cm^{-1}), and Al–O–Si (540 cm^{-1}) [43]. The XRD peaks at 12.4° , 25.0° , and 45.7° for kaolinite and at 20.0° , 26.7° , 35.1° , 38.4° , 55.0° and 62.5° for HAL are present in both sample types. SEM images of HAL after Co^{2+} adsorption show the tubular structure characteristics. However, EDS analysis results indicate the presence of the Co^{2+} elemental spectrum in the HAL powder after adsorption. These results suggest that HAL material has successfully adsorbed Co^{2+} ions. However, due to the limited amount of adsorbed ions, it has not significantly affected the morphology of the HAL mineral, as well as the FT-IR and XRD analysis results.

**Figure 4:** FT-IR spectra (a) and XRD pattern (b) of HAL before and after Co^{2+} adsorption process.

3.1.7 Adsorption isotherm

In each experiment, 0.8 g of HAL was used to adsorb Co^{2+} ions in a 50 mL solution with varying initial concentrations. The adsorption process was conducted at the natural pH of 6.09 and room temperature (25°C) for 80 min. The remaining Co^{2+} concentration at equilibrium (C_e) was determined, and the adsorption capacity (Q) was calculated (Table 3). The Langmuir and Freundlich isotherm equations were constructed using Eqs. 3 and 4, respectively. The experimental data were plotted on the adsorption isotherm graphs (Figure 6). The Langmuir isotherm equation represents the maximum adsorption capacity (Q_m) and the Langmuir constant (K_L), while the Freundlich equation involves the experimental constants K_F and n . The results presented in Table 4 indicate that the adsorption of Co^{2+} on HAL follows the Langmuir isotherm adsorption model ($R^2 = 0.98113$, Sum of the Square of the Errors (SSE) = 0.07672). This finding is consistent with numerous published results that have utilized HAL as an adsorbent for heavy metals and organic pigments [4]. The Langmuir isotherm model provides insights

into the maximum adsorption capacity (3.10206) and the interaction between the adsorbate (Co^{2+} ions) and the adsorbent (HAL) during adsorption.

3.1.8 Adsorption kinetic

The adsorption kinetic was studied based on the effect of adsorption time on the Co^{2+} adsorption capacity by constructing graphs of the pseudo-first-order (Eq. 5) and pseudo-second-order kinetics (Eq. 6). The resulting graphs in Figure 7 exhibited non-linear lines for the pseudo-first-order and pseudo-second-order modes. The regression coefficients (R^2), adsorption rate constants (k) and the adsorption capacity at equilibrium (Q_e) were determined in Table 5. The results indicated that the regression coefficient of the pseudo-second-order kinetic equation ($R^2 = 0.94315$) was much higher than that of the pseudo-first-order kinetic equation ($R^2 = 0.67314$) as well as the lower value of the SSE of the pseudo-second-order kinetic equation (SSE = 0.01223) than the pseudo-first-order kinetic equation (SSE = 0.07033). This result confirms that

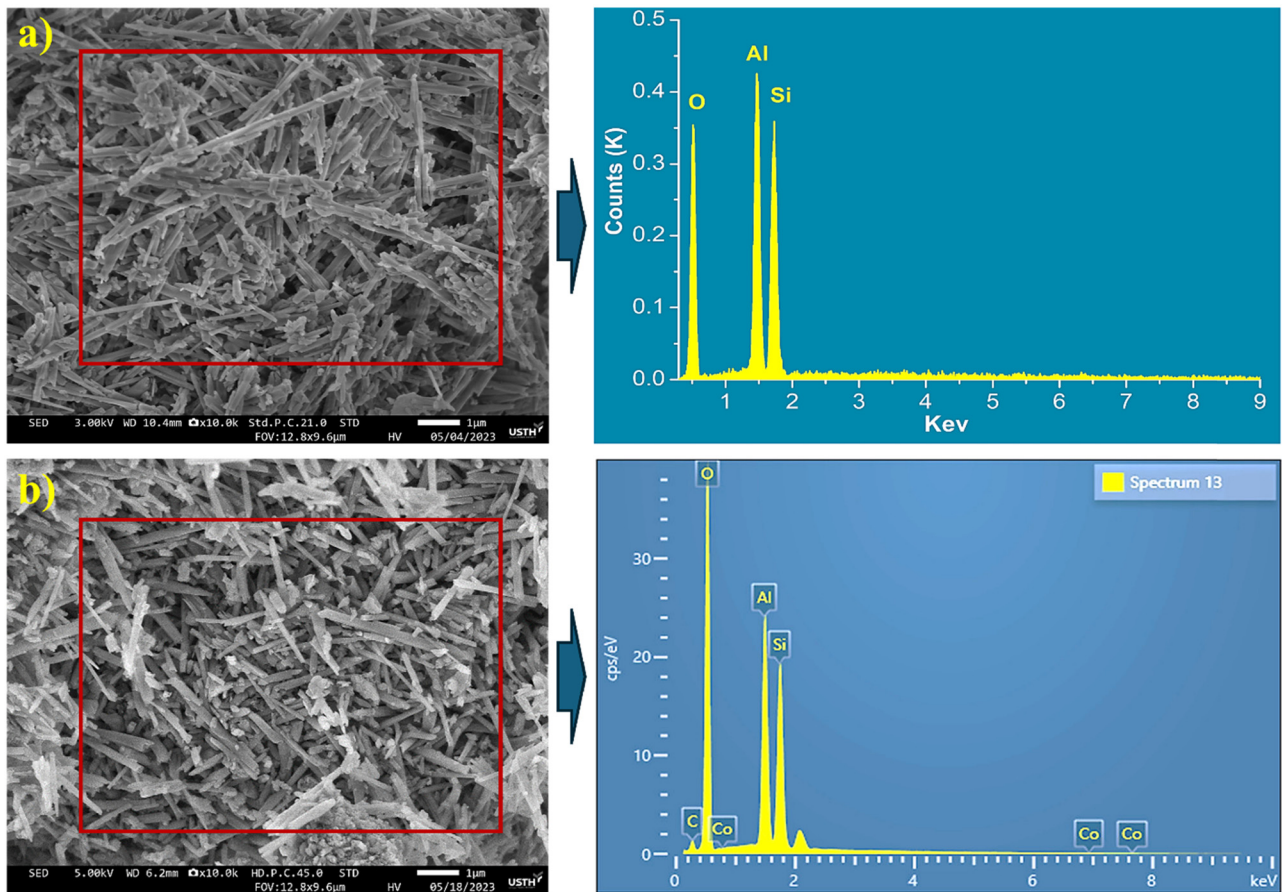


Figure 5: SEM images and EDX results of HAL before (a) and after (b) Co^{2+} adsorption process.

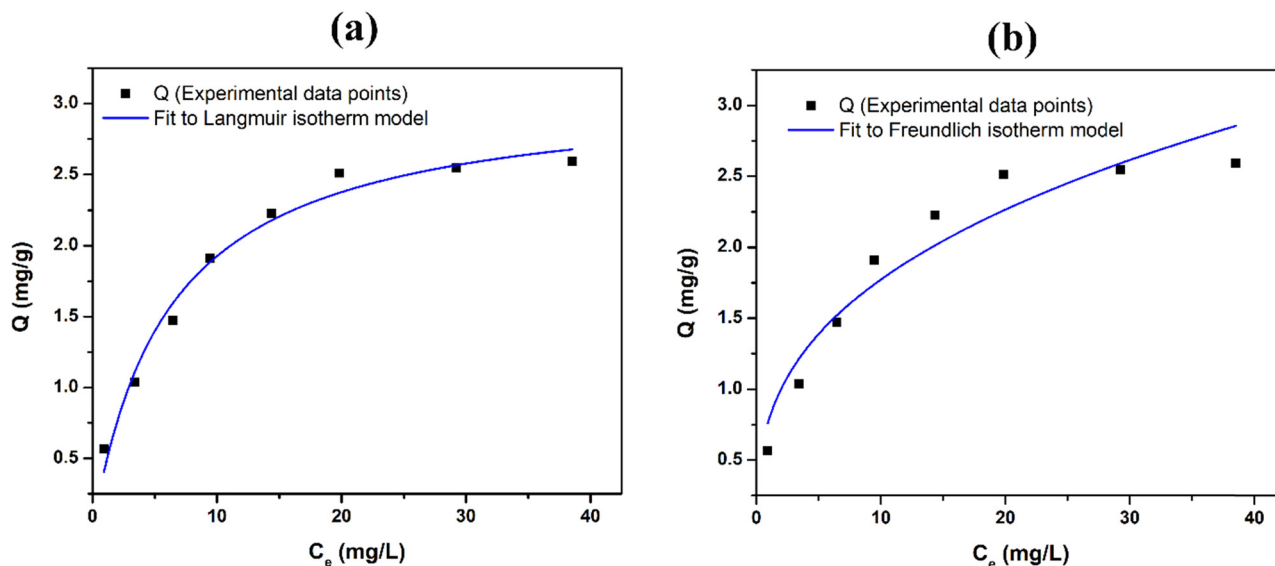


Figure 6: Langmuir (a) and Freundlich (b) isotherm plots for the adsorption of Co^{2+} onto HAL.

the adsorption of Co^{2+} by HAL follows the pseudo-second-order adsorption kinetic. The adsorption rate constant, k , was calculated to be $0.13905 \text{ g}\cdot\text{mg}^{-1}\cdot\text{min}^{-1}$. This indicates that the pseudo-second-order kinetic model better describes the adsorption process, which suggests a chemisorption mechanism involving strong bonding between the adsorbate (Co^{2+} ions) and the adsorbent (HAL).

3.2 Desorption of Co^{2+} out of Co-HAL and recovery of Co metal by electrodeposition method

3.2.1 Cyclic voltammograms (CVs) of $\text{Co}(\text{NO}_3)_2$ and Co-HAL in the electrolyte of reline solvent

The results shown in Figure 8a demonstrate the presence of a reduction peak of Co^{2+} at -1.25 V and an oxidation peak of Co^0 at -0.35 V in the cyclic voltammetry curve of reline containing $\text{Co}(\text{NO}_3)_2$. This observation aligns with the reported CV of reline having Co^{2+} in the literature [34,37]. Figure 8b presents the results of the cyclic voltammetry curve of reline

containing Co-HAL, showing a reduction peak of Co^{2+} at -1.3 V and an oxidation peak of Co^0 at -0.55 V . These results indicate a slight shift in the oxidation-reduction peaks of cobalt between $\text{Co}(\text{NO}_3)_2/\text{reline}$ and $\text{Co-HAL}/\text{reline}$. The mechanism of the deposition and dissolution of cobalt on the Au electrode can be described as follows:

Step 1: The formation of a complex between Co^{2+} from Co-HAL and Cl^- from reline occurs, forming CoCl_n^{2-n} . Subsequently, the reduction of Co^{2+} (of CoCl_n^{2-n}) takes place on the surface of the electrode, leading to the formation of metallic Co: $\text{CoCl}_n^{2-n} + 2e \rightarrow \text{Co} + n\cdot\text{Cl}^-$

Step 2: Stripping of the Co metal occurs, converting it back to Co^{2+} : $\text{Co} - 2e \rightarrow \text{Co}^{2+}$

The cyclic voltammetry result of Co-HAL in reline solvent suggests that Co^{2+} ions can be effectively desorbed from the Co-HAL material and subsequently reduced to metallic Co on the surface of the Au electrode in the reline solvent. This electrochemical process allows for the recovery of the HAL adsorbent. The deposition of Co metal on the Au electrode surface can be achieved at a potential equal or less than -1.3 V . This possible range ensures the successful electrochemical recovery of Co from the Co-HAL material.

Table 4: Adsorption isotherm parameters

Q_m	Langmuir			Freundlich			
	K_L	R^2	SSE	$1/n$	K_F	R^2	SSE
3.10206 ± 0.13551	0.16371 ± 0.0239	0.98113	0.07672	0.35363 ± 0.049	0.78519 ± 0.11591	0.78519	0.27993

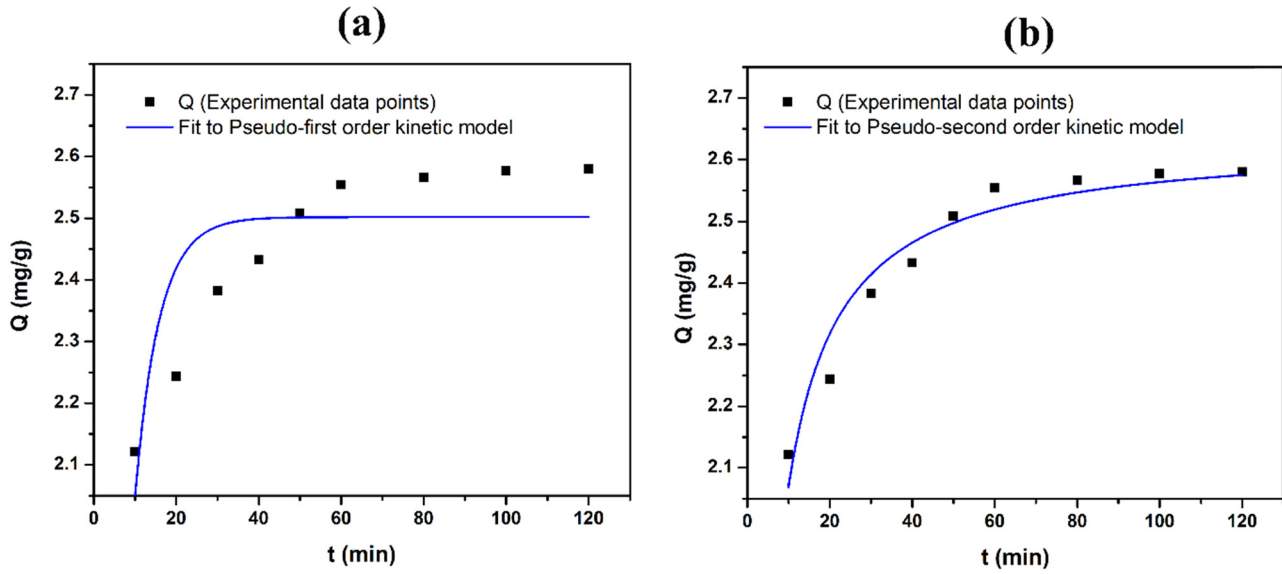


Figure 7: Isotherm plots for the adsorption of Co^{2+} onto HAL according to pseudo-first-order kinetic equation (a) and pseudo-second-order kinetic equation (b).

Table 5: Adsorption kinetic parameters

Pseudo-first-order kinetic equation				Pseudo-second-order kinetic equation			
Q_e ($\text{mg}\cdot\text{g}^{-1}$)	k_1 (min^{-1})	R^2	SSE	Q_e ($\text{mg}\cdot\text{g}^{-1}$)	k_2 ($\text{g}\cdot\text{mg}^{-1}\cdot\text{min}^{-1}$)	R^2	SSE
2.50211	0.1703	0.67314	0.07033	2.63375	0.13905	0.94315	0.01223

3.2.2 Effect of applied current and electrolytic time on recovery efficiency of cobalt

The recovery of cobalt was achieved through the electrodeposition method using the applied current technique. Figure 9 illustrates the process of cobalt deposition into

the reline solvent through electrodeposition at the applied current of 7.5 mA. The potential reached -1.5 V and was quite stable during the electrolysis process.

The initial smooth surface of the Au electrode can be observed in Figure 10a. EDX spectroscopy analysis of the Au electrode confirmed the presence of characteristic

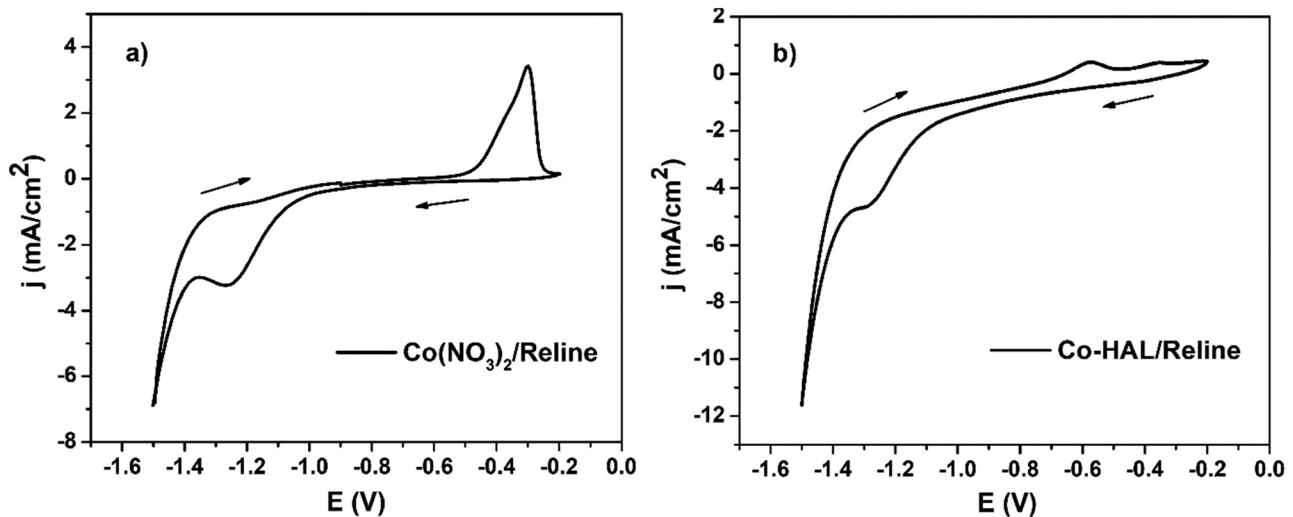


Figure 8: CV of 0.005 M Co^{2+} in the reline. A scan rate of $50\text{ mV}\cdot\text{S}^{-1}$, $T = 60^\circ\text{C}$ (a). CV of 5 mL reline containing 1.2 g Co-HAL . Scan rate of $50\text{ mV}\cdot\text{S}^{-1}$, $T = 60^\circ\text{C}$ (b).

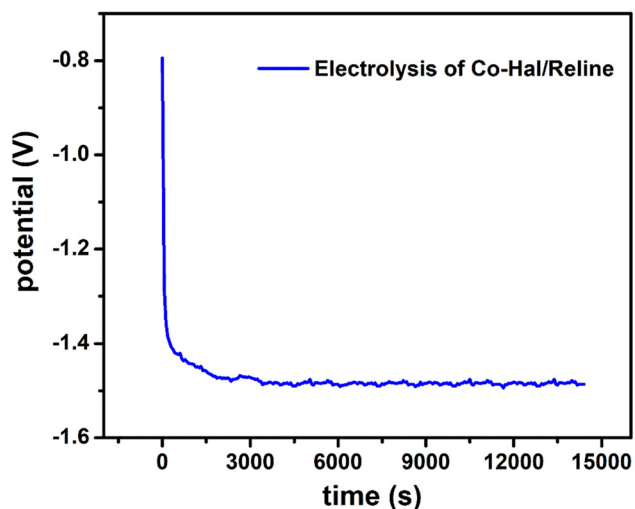


Figure 9: Electrolysis of 5 mL reline containing 0.5 g Co-HAL at 7.5 mA applied current, scan rate of $50 \text{ mV}\cdot\text{s}^{-1}$, electrolytic time of 4 h, and $T = 60^\circ\text{C}$.

peaks corresponding to Au, aluminum (Al), and silicon (Si), which are components of the Au electrode. After the electrolysis process, a uniform deposition of Co metal was

Table 6: Recovery efficiency of Co (H %) from 0.5 g Co-HAL at different applied currents and electrolytic times

t (h)	H%			
	I (mA)			
	2	3	5	7.5
1	62.11	68.69	74.60	81.34
2	72.38	76.11	82.91	87.00
3	76.08	78.86	84.67	90.12
4	78.62	81.70	86.47	92.05
5	80.33	85.68	89.25	94.11

observed on the surface of the Au electrode, as shown in Figure 10b. The EDX spectroscopy analysis of the electrode after electrolysis still indicated the presence of Co metal, confirming the successful electrodeposition of Co onto the Au electrode. To assess the recovery efficiency of Co, cathodic polarization of the Au electrode was conducted at different applied current values and electrolytic times at a temperature of 60°C . The results of the recovery efficiency of Co are presented in Table 6, providing valuable

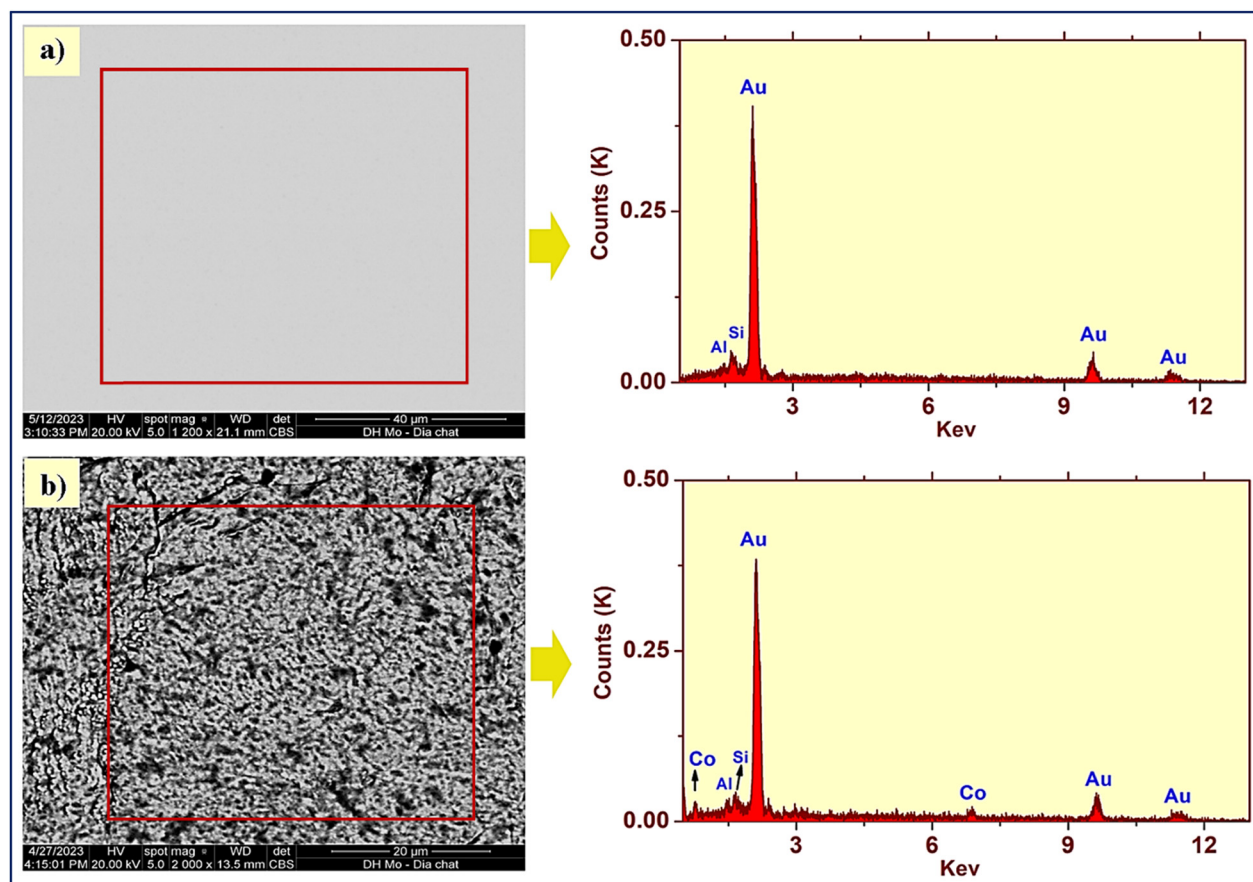


Figure 10: SEM-EDX of the surface of the Au electrode before (a) and after (b) electrolysis.

insights into the effectiveness of the electrodeposition method for Co recovery.

The results presented in Table 6 demonstrate the variation in the recovery efficiency of Co based on the applied current and electrolytic time. It was observed that increasing the applied current resulted in a higher amount of Co being deposited on the surface of the Au electrode, leading to an increase in the recovery efficiency of Co. Similarly, increasing the electrolytic time also led to a higher amount of Co deposition and an increase in the recovery efficiency of Co. Notably, the recovery efficiency of Co reached 94.11% after 5 h of electrolysis at an applied current of 7.5 mA. This indicates that a significant amount of Co was successfully recovered from the Co-HAL material and deposited onto the surface of the Au electrode. These findings highlight the effectiveness of the electrodeposition method in the recovery of Co, with higher applied current and longer electrolytic time contributing to higher recovery efficiency and more significant deposition of Co metal.

3.2.3 Regeneration of HAL material

During the electrolysis process, Co^{2+} ions were successfully desorbed from the Co-HAL material, allowing for the recovery of HAL material for further adsorption applications. Figure 11 presents the XRD pattern of the HAL material obtained after electrolysis, which closely resembles the XRD pattern of the initial HAL material. This indicates that

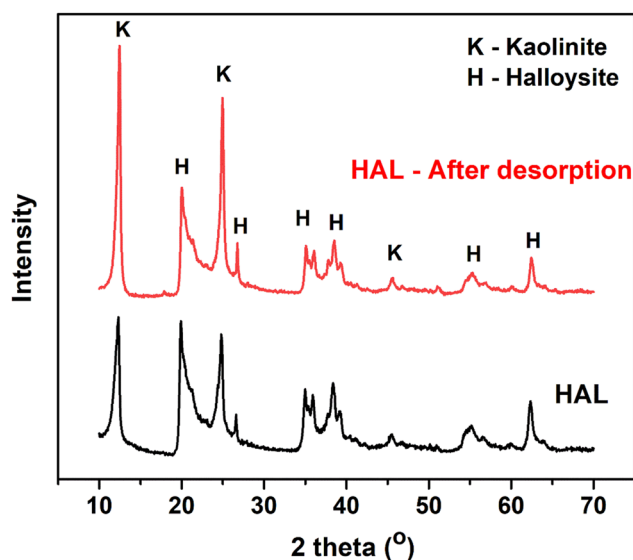


Figure 11: XRD patterns of HAL before Co^{2+} adsorption and after the desorption process.

the electrolysis process did not significantly alter the crystal structure of the HAL material. To assess the regeneration ability of the prepared sorbent, adsorption experiments were conducted under suitable conditions. After electrolysis, the obtained HAL material exhibited a Co^{2+} adsorption capacity (Q) of $1.55 \text{ mg}\cdot\text{g}^{-1}$ and an adsorption efficiency (H) of 61.56%. This indicates that the regenerated HAL material retains a significant adsorption capacity and efficiency for Co^{2+} ions. These results suggest that the electrolysis process effectively desorbs Co^{2+} ions from the HAL material, allowing the sorbent's successful recovery and reuse for subsequent adsorption processes.

4 Conclusion

HAL clay has shown a high efficiency of 76.36% in removing Co^{2+} ions from aqueous solutions. The equilibrium time for the adsorption process was determined to be 80 min. The adsorption isotherm results indicated that the adsorption of Co^{2+} ions using HAL powder followed the Langmuir isotherm model, with a maximum monolayer adsorption capacity of $2.992 \text{ mg}\cdot\text{g}^{-1}$. The adsorption kinetics data confirmed that the adsorption process of Co^{2+} ions on HAL powder followed the pseudo-second-order kinetic model, with a high correlation coefficient (R^2) of 0.9998. This indicates that the adsorption process is well-described by this kinetic model. The recovery of cobalt from the adsorbed HAL material was achieved through electrodeposition on the surface of an Au electrode. A recovery efficiency of 94.11% was achieved after 5 h of electrolysis at an applied current density of 7.5 mA in the reline electrolytic solution. Significantly, the HAL adsorbent was not dissolved during the electrolysis process, demonstrating its stability and the possibility of regeneration. The obtained HAL material after desorption exhibited an adsorption capacity of $1.55 \text{ mg}\cdot\text{g}^{-1}$ and an adsorption efficiency of 61.56%. This indicates that the HAL adsorbent can be successfully reused after the desorption process, making it a sustainable and cost-effective solution for heavy metal removal from aqueous solutions.

Funding information: The authors express their gratitude for the financial support provided by the Ministry of Education and Training (project code: B2022-MDA-03), which has played a crucial role in completing this work.

Author contributions: All authors contributed equally to this article.

Conflict of interest: Authors state no conflict of interest.

Data availability statement: The datasets generated during and/or analyzed during the current study are available from the corresponding author on reasonable request.

References

- [1] Joussein E, Petit S, Churchman GJ, Theng BKG, Righi D, Delvaux B. Halloysite clay minerals – A review. *Clay Min.* 2005;40:383–426. doi: 10.1180/0009855054040180.
- [2] Yuan P, Tan D, Annabi-Bergaya F. Properties and applications of halloysite nanotubes: Recent research advances and future prospects. *Appl Clay Sci.* 2015;112–113:75–93. doi: 10.1016/j.clay.2015.05.001.
- [3] Zhang Y, Tang A, Yang H, Ouyang J. Applications and interfaces of halloysite nanocomposites. *Appl Clay Sci.* 2016;119:8–17. doi: 10.1016/j.clay.2015.06.034.
- [4] Anastopoulos I, Mittal A, Usman M, Mittal J, Yu G, Núñez-Delgado A, et al. A review on halloysite-based adsorbents to remove pollutants in water and wastewater. *J Mol Liq.* 2018;269:855–68. doi: 10.1016/j.molliq.2018.08.104.
- [5] Danyliuk N, Tomaszewska J, Tatarchuk T. Halloysite nanotubes and halloysite-based composites for environmental and biomedical applications. *J Mol Liq.* 2020;309:113077. doi: 10.1016/j.molliq.2020.113077.
- [6] Maziarz P, Matusik J. The effect of acid activation and calcination of halloysite on the efficiency and selectivity of Pb(II), Cd(II), Zn(II) and As(V) uptake. *Clay Min.* 2016;51:385–94. doi: 10.1180/claymin.2016.051.3.06.
- [7] Parisi F, Lazzara G, Merli M, Milioto S, Princivalle F, Sciascia L. Simultaneous Removal and Recovery of Metal Ions and Dyes from Wastewater through Montmorillonite Clay Mineral. *Nanomaterials.* 2019;9:1699. doi: 10.3390/nano9121699.
- [8] Kurczewska J, Cegłowski M, Schroeder G. Alginate/PAMAM dendrimer - Halloysite beads for removal of cationic and anionic dyes. *Int J Biol Macromol.* 2019;123:398–408. doi: 10.1016/j.ijbiomac.2018.11.119.
- [9] Maziarz P, Matusik J, Radziszewska A. Halloysite-zero-valent iron nanocomposites for removal of Pb(II)/Cd(II) and As(V)/Cr(VI): Competitive effects, regeneration possibilities and mechanisms. *J Environ Chem Eng.* 2019;7:103507. doi: 10.1016/j.jece.2019.103507.
- [10] Pirhaji ZJ, Moeinpour F, Dehabadi MA, Ardakani YAS. Synthesis and characterization of halloysite/graphene quantum dots magnetic nanocomposite as a new adsorbent for Pb(II) removal from water. *J Mol Liq.* 2020;300:112345. doi: 10.1016/j.molliq.2019.112345.
- [11] Ramanayaka S, Sarkar B, Coorayc TA, Oke YS, Vithanage M. Halloysite nanoclay supported adsorptive removal of oxytetracycline antibiotic from aqueous media. *J Hazard Mater.* 2020;384:121301. doi: 10.1016/j.jhazmat.2019.121301.
- [12] Li H, Sheng G, Teppen JB, Johnston TC, Boyd AS. Sorption and desorption of pesticides by clay minerals and humic acid-clay complexes. *Soil Sci Soc Am J.* 2003;67:120–31. doi: 10.2136/sssaj2003.0122.
- [13] Kushwaha J, Singh R. Cellulose hydrogel and its derivatives: A review of application in heavy metal adsorption. *Inorg Chem Commun.* 2023;152:110721. doi: 10.1016/j.inoche.2023.110721.
- [14] Jiang H, Wu S, Zhou J. Preparation and modification of nanocellulose and its application to heavy metal adsorption: A review. *Int J Biol Macromol.* 2023;236:123916. doi: 10.1016/j.ijbiomac.2023.123916.
- [15] Xu K, Li L, Huang Z, Tian Z, Li H. Efficient adsorption of heavy metals from wastewater on nanocomposite beads prepared by chitosan and paper sludge. *Sci Total Environ.* 2022;846:157399. doi: 10.1016/j.scitotenv.2022.157399.
- [16] Amin FK, Gulshan F, Asrafuzzaman F, Das H, Rashid R, Hoque SM. Synthesis of mesoporous silica and chitosan-coated magnetite nanoparticles for heavy metal adsorption from wastewater. *Environ Nanotechnol Monit Manag.* 2023;20:100801. doi: 10.1016/j.enmm.2023.100801.
- [17] Liu X, Yin H, Liu H, Cai Y, Qi X, Dang Z. Multicomponent adsorption of heavy metals onto biogenic hydroxyapatite: Surface functional groups and inorganic mineral facilitating stable adsorption of Pb (II). *J Hazard Mater.* 2023;443:130167. doi: 10.1016/j.jhazmat.2022.130167.
- [18] Yang S, Yang G. Origin for superior adsorption of metal ions and efficient control of heavy metals by montmorillonite: A molecular dynamics exploration. *Chem Eng J Adv.* 2023;14:100467. doi: 10.1016/j.cej.2023.100467.
- [19] Li H, Zhang J, Zhang Y, Huang H, Ou H, Zhang Y. In-situ adsorption-conversion recovery of heavy metal cadmium by natural clay mineral for multi-functional photocatalysis. *Sep Purif Technol.* 2023;319:124058. doi: 10.1016/j.seppur.2023.124058.
- [20] Wu Y, Ming J, Zhou W, Xiao N, Cai J. Efficiency and mechanism in preparation and heavy metal cation/anion adsorption of amphoteric adsorbents modified from various plant straws. *Sci Total Environ.* 2023;884:163887. doi: 10.1016/j.scitotenv.2023.163887.
- [21] Peld M, Tõnsuaadu K, Bender V. Sorption and desorption of Cd²⁺ and Zn²⁺ ions in apatite-aqueous systems. *Environ Sci Technol.* 2004;38:5626–31. doi: 10.1021/es049831l.
- [22] Smičiklas I, Dimović S, Plečaš I, Mitrić M. Removal of Co²⁺ from aqueous solutions by hydroxyapatite. *Water Res.* 2006;40:2267–74. doi: 10.1016/j.watres.2006.04.031.
- [23] Zhu R, Yu R, Yao J, Mao D, Xing C, Wang D. Removal of Cd²⁺ from aqueous solutions by hydroxyapatite. *Catal Today.* 2008;139:94–99. doi: 10.1016/j.cattod.2008.08.011.
- [24] Chen J-H, Wang Y-J, Zhou D-M, Cui Y-X, Wang S-Q, Chen Y-C. Adsorption and desorption of Cu(II), Zn(II), Pb(II), and Cd(II) on the soils amended with nanoscale hydroxyapatite. *Environ Prog Sustain Energy.* 2010;29(2):233–41. doi: 10.1002/ep.10371.
- [25] Zhang W, Wang F, Wang P, Lin L, Zhao Y, Zou P, et al. Facile synthesis of hydroxyapatite/yeast biomass composites and their adsorption behaviors for lead (II). *J Colloid Interface Sci.* 2016;477:181–90. doi: 10.1016/j.jcis.2016.05.050.
- [26] Kede MLFM, Mavropoulos E, da Rocha NCC, Costa AM, Prado da Silva MH, Moreira JC, et al. Polymeric sponges coated with hydroxyapatite for metal immobilization. *Surf Coat Technol.* 2012;206:2810–6. doi: 10.1016/j.surfcoat.2011.11.044.
- [27] Chand P, Pakade YB. Synthesis and characterization of hydroxyapatite nanoparticles impregnated on apple pomace to enhanced adsorption of Pb(II), Cd(II), and Ni(II) ions from aqueous solution. *Environ Sci Pollut Res.* 2015;22:10919. doi: 10.1007/s11356-015-4276-2.
- [28] Itami K, Yanai J. Sorption and desorption properties of cadmium and copper on soil clays in relation to charge characteristics. *Soil Sci Plant Nutr.* 2006;52:5–12. doi: 10.1111/j.1747-0765.2006.00015.x.
- [29] Helios Rybicka E, Calmano W, Breeger A. Heavy metals sorption/desorption on competing clay minerals: an experimental study. *Appl Clay Sci.* 1995;9:369–81. doi: 10.1016/0169-1317(94)00030-T.

- [30] Quaghebeur M, Rengel Z, Rate AW, Hinz C. Heavy metals in the environment desorption kinetics of arsenate from kaolinite as influenced by pH. *J Environ Qual.* 2005;34:479–86.
- [31] Ma F-Q, Zhu W-M, Cheng W-T, Chen J-Q, Gao J-Z, Xue Y, et al. Removal of cobalt ions (II) from simulated radioactive effluent by electrosorption on potassium hydroxide modified activated carbon fiber felt. *J Water Process Eng.* 2023;53:103635. doi: 10.1016/j.jwpe.2023.103635.
- [32] Kyzas GZ, Deliyanni EA, Matis KA. Activated carbons produced by pyrolysis of waste potato peels: Cobalt ions removal by adsorption. *Colloids Surf A Physicochem Eng Asp.* 2016;490:74–83. doi: 10.1016/j.colsurfa.2015.11.038.
- [33] Silva PAP, Oréface RL. Biosorbent from castor oil polyurethane foam containing cellulose-halloysite nanocomposite for removal of manganese, nickel and cobalt ions from water. *J Hazard Mater.* 2023;454:131433. doi: 10.1016/j.jhazmat.2023.131433.
- [34] Pereira NM, Brincoveanu O, Pantazi AG, Pereira CM, Araújo JP, Silva AF, et al. Electrodeposition of Co and Co composites with carbon nanotubes using choline chloride-based ionic liquids. *Surf Coat Technol.* 2017;324:451–62. doi: 10.1016/j.surfcoat.2017.06.002.
- [35] Chua Q-W, Liang J, Hao J-C. Electrodeposition of zinc-cobalt alloys from choline chloride-urea ionic liquid. *Electrochim Acta.* 2014;115:499–503. doi: 10.1016/j.electacta.2013.10.204.
- [36] You Y-H, Gu C-D, Wang X-L, Tu J-P. Electrodeposition of Ni-Co alloys from a deep eutectic solvent. *Surf Coat Technol.* 2012;206:3632–8. doi: 10.1016/j.surfcoat.2012.03.001.
- [37] Gómez E, Cojocarú P, Magagnin L, Valles E. Electrodeposition of Co, Sm and SmCo from a Deep Eutectic Solvent. *J Electroanal Chem.* 2011;658:18–24. doi: 10.1016/j.jelechem.2011.04.015.
- [38] Neha G, Atul K, Chattopadhyaya MC. Adsorption studies of cationic dyes onto Ashoka (*Saraca asoca*) leaf powder. *J Taiwan Inst Chem Eng.* 2012;43:604–13. doi: 10.1016/j.jtice.2012.01.008.
- [39] Rabbat C, Pinna A, Andres Y, Villot A, Awad S. Adsorption of ibuprofen from aqueous solution onto a raw and steam-activated biochar derived from recycled textiles insulation panels at end-of-life: Kinetic, isotherm and fixed-bed experiments. *J Water Process Eng.* 2023;53:103830. doi: 10.1016/j.jwpe.2023.103830.
- [40] Dou W-S, Deng Z-P, Fan J-P, Lin Q-Z, Wu Y-H, Ma Y-L, et al. Enhanced adsorption performance of La(III) and Y(III) on kaolinite by oxalic acid intercalation expansion method. *Appl Clay Sci.* 2022;229:106693. doi: 10.1016/j.clay.2022.106693.
- [41] Abdel-Fadeel MA, Aljohani NS, Al-Mhyawi SR, Halawani RF, Aljuhani EH, Salam MA. A simple method for removal of toxic dyes such as Brilliant Green and Acid Red from the aquatic environment using Halloysite nanoclay. *J Saudi Chem Soc.* 2022;26:101475. doi: 10.1016/j.jscs.2022.101475.
- [42] Aljohani NS, Kavil YN, Al-Farawati RK, Alelyani SS, Orif MI, Shaban YA, et al. The effective adsorption of arsenic from polluted water using modified Halloysite nanoclay. *Arab J Chem.* 2023;16:104652. doi: 10.1016/j.arabjc.2023.104652.
- [43] Bui HB, Hoang N, Nguyen TTT, Le TD, Vo TH, Nguyen TD, et al. Performance evaluation of nanotubular halloysites from weathered pegmatites in removing heavy metals from water through novel artificial intelligence-based models and human-based optimization algorithm. *Chemosphere.* 2021;282:131012. doi: 10.1016/j.chemosphere.2021.131012.